


Well-Defined Au/ZnO Nanoparticle Composites Exhibiting Enhanced Photocatalytic Activities

Nayane Udawatte,[†] Myeongsoon Lee,[‡] Junhyung Kim,[‡] and Dongil Lee^{*,‡}

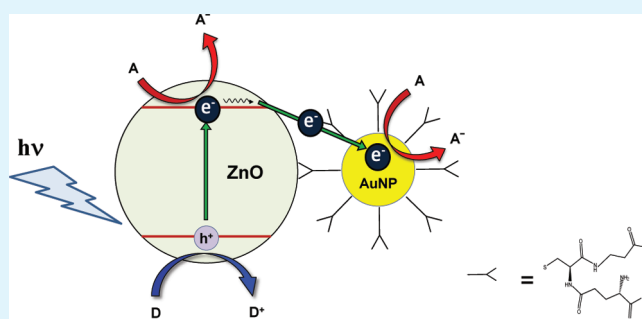
[†]Department of Chemistry, Western Michigan University, Kalamazoo, Michigan 49008, United States

[‡]Department of Chemistry, Yonsei University, Seoul 120-749, Korea

 Supporting Information

ABSTRACT: Well-defined Au/ZnO nanoparticle composites were prepared by modifying ZnO with preformed Au nanoparticles protected with bifunctional glutathione ligand. In this approach, the Au nanoparticles were highly monodisperse and their loading on ZnO surface could be precisely controlled by the anchoring conditions. Steady-state and time-resolved photoluminescence of the composites revealed the ability of the Au nanoparticles to efficiently extract conduction band electrons from the photoexcited ZnO. The composites exhibited strongly enhanced photocatalytic activity without requiring thermal activation process in degrading organic substrates in both oxidative and reductive pathways. A clear correlation between the photocatalytic activity and the Au loading was found for both oxidative and reductive photocatalytic reactions. These results demonstrate that thiolate-protected AuNPs can significantly enhance the charge separation by extracting electrons from the photoexcited ZnO and consequently improve the photocatalytic activity of the composites.

KEYWORDS: nanocomposite, ZnO, Au nanoparticle, photocatalysis, photoluminescence, glutathione, rhodamine, thionine



INTRODUCTION

The demonstration of the photocatalytic water splitting on TiO₂ electrodes revealed¹ the potential of semiconductors to be used as heterogeneous photocatalysts, and extensive research has since been performed in understanding the fundamental processes of semiconductor photocatalysis. It has been found that up to 90% of photogenerated charge carriers may undergo recombination,² consequently adversely affecting the photocatalytic efficiency of semiconductor materials. The use of nanosized semiconductor particles is advantageous^{3–5} in this regard because of the increased number of catalytically active sites and the reduced charge recombination in bulk, resulting from the large surface to volume ratio of the nanoparticles. Significant enhancement of photocatalytic efficiency can be achieved additionally by the deposition of noble metal nanoparticles,⁶ such as Au or Pt on the semiconductor nanoparticle surfaces, because metal can act as a reservoir for photogenerated electrons,⁷ thereby promoting interfacial charge separation processes.

A number of methods for the deposition of metal nanoparticles on semiconductor surfaces have been demonstrated including coprecipitation, deposition–precipitation and chemical vapor deposition.^{8,9} However, these methods often led to problems, for example, embedding of metal in the bulk instead of the surface of the semiconductor,¹⁰ incorporation of foreign ions such as Cl[−],¹¹ and metal deposits with a wide size distribution.^{6,12} Use of monodisperse metal nanoparticles is

especially important as chemical and physical properties of nanoparticles are critically dependent upon the particle dimensions in the nanometer scale.^{13,14}

Alternatively, anchoring of preformed metal nanoparticles on semiconductor surfaces is advantageous, in which particle size could be controlled independently and very narrow size distributions could be obtained via well-established synthetic methods.¹⁵ In a previous study,^{16,17} we have shown that structurally well-defined composite photocatalysts could be prepared by modification of TiO₂ with thiolate-protected gold nanoparticles. The photocatalytic activity of the composite, however, exhibited essentially no enhancement with gold modification and thus thermal treatment of the composite was used to activate the catalytic activity.

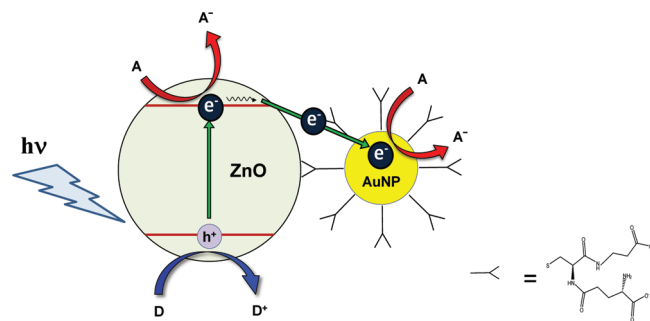
ZnO exhibits a band gap of 3.4 eV and an electronic affinity of 4.2 eV, similar to those of TiO₂, and thus is considered to be a viable alternative to TiO₂ in dye-sensitized solar cells and photocatalysts.^{18–20} Herein, we present the preparation and photocatalytic activity of a well-defined composite based on ZnO modified with thiolate-protected gold nanoparticles (AuNPs). Highly monodisperse AuNPs were synthesized via a facile synthetic method and the AuNPs were assembled onto ZnO nanoparticles

Received: September 9, 2011

Accepted: October 26, 2011

Published: October 26, 2011

Scheme 1. Schematic Illustration (Not to Scale) of Photoexcitation, Electron Transfer, and Photocatalytic Reactions at a ZnO–AuNP Composite (A, electron acceptor; D, electron donor)



using a bifunctional glutathione linker as illustrated in Scheme 1. Photoexcitation of ZnO generates holes in the valence band and electrons in the conduction band of ZnO. When AuNPs are present on the surface of ZnO, the AuNPs would act as an electron sink and thus could greatly enhance the charge separation efficiency. Consequently, it is expected that more electrons and holes become available for subsequent catalytic reactions. The ZnO–AuNP composite catalysts were found to exhibit strongly enhanced photocatalytic activity toward both oxidation and reduction of substrates without requiring any thermal treatment step, in contrast to most of the similar photocatalysts reported in the literature where enhancement of photocatalytic activity was only achieved after some form of heat treatment.^{16,21,22} Strong correlation between the photocatalytic activity and the AuNP loading was observed, demonstrating the active role AuNPs in the photocatalytic reaction of the composites.

EXPERIMENTAL METHODS

Chemicals. L-Glutathione reduced (GSH, >99%), sodium borohydride (NaBH_4 , 99%), hydrogen tetrachloroaurate trihydrate ($\text{HAuCl}_4 \cdot 3\text{H}_2\text{O}$, ACS reagent grade), zinc oxide nanoparticles (ZnO, 99.9%), thionine acetate (TH, >85%), methanol (99.9%) and acetonitrile (99.9%) were purchased from Sigma-Aldrich. Rhodamine 6G (R6G, 99%) was purchased from Exciton. All chemicals were used as received without further purification. Ultrapure water with a resistivity of 18.2 M Ω cm was obtained from a Millipore Milli-Q system.

Synthesis of Glutathione-Protected AuNPs. A modified literature procedure was utilized to synthesize glutathione-protected AuNPs.²³ 1 mmol (0.39 g) of HAuCl_4 was dissolved in a solution of 30 mL of methanol and 20 mL of water, which resulted in a bright yellow solution. One mmol (0.31 g) of glutathione is added to the rapidly stirred gold salt solution. The solution turned light brown and slowly turned colorless within 40 min. A NaBH_4 solution, freshly made by dissolving 5 mmol (0.19 g) of NaBH_4 in 40 mL of water, was slowly added to the vigorously stirred precursor solution, which caused the solution to immediately turn dark brown due to the formation of gold nanoparticles. The solution was quickly transferred into a water bath that was kept at 50 °C, and stirring was continued for 1 h. The resulting solution was evaporated to near dryness on a rotary evaporator at 30 °C. Excess methanol was added to precipitate particles and wash reaction byproducts and any remaining starting material. The washed product consisted of AuNPs with various sizes. The product was dissolved in 20 mL of water and then 4 mL of methanol was added to induce precipitation of

AuNPs. After removing the AuNP precipitate (the largest AuNP) by centrifugation, the supernatant was treated with more methanol to induce further precipitation. This recrystallization procedure was repeated with increasing amounts of methanol until a clear supernatant was obtained. Various sized AuNPs were isolated from this recrystallization process. The AuNPs thus obtained were reasonably monodisperse in size, and the second isolate with an average core diameter of 3.4 ± 0.6 nm was used for the subsequent photocatalytic investigations.

Preparation and Characterization of ZnO–AuNP Composites. The composites were prepared by anchoring the glutathione-protected AuNPs on the surfaces of ZnO nanoparticles. Commercially available ZnO nanoparticles with a primary particle size <100 nm and BET surface area of 15–25 m²/g were used. The AuNP anchoring process was carried out by stirring ZnO with a predetermined amount of AuNPs in water for 5 h. The composites were isolated by centrifugation, and were dried in vacuum. The resulting ZnO–AuNP composites containing 0.4, 0.7, 1, and 2 wt % glutathione-protected AuNP relative to ZnO are referred to 0.4, 0.7, 1, and 2 wt % composite, respectively.

Transmission electron microscopy (TEM) images were acquired with a JEOL 2100F operating at 200 kV. The samples were prepared by drop casting of a sample solution onto 400 mesh Formvar/carbon coated copper grids (FCF400-CU, Electron Microscopy Sciences). Optical absorption spectra were obtained with a Perkin-Elmer Lambda 40 spectrophotometer.

An aqueous suspension of ZnO or ZnO–AuNP composite with a concentration of 0.1 g/L was used for steady-state photoluminescence (PL) measurements. PL was measured using a FL920 spectrofluorimeter (Edinburgh Instruments) with photoexcitation wavelength set at 330 nm. Time-resolved PL measurements were made with concentrated 1 g/L solutions of ZnO or 2 wt % composite using a femtosecond fluorescence upconversion system (CDP Instruments, Inc., Russia) described elsewhere.²⁴ The present measurements were carried out with 267 nm excitation (fundamental of Ti:sapphire was set at 800 nm) and decay traces of the band edge emissions were obtained at 375 nm. Instrument response function (IRF) was measured using the rise time of several dye molecules, which gave a sigma value of ~ 290 fs. Stability of the samples was verified by repetition and only little degradation was observed because of laser excitation.

Photocatalysis Experiments. For the photocatalytic experiments performed under atmospheric conditions, a catalyst suspension (ZnO or composites) in water and an aqueous solution of the substrate R6G were mixed in a 1 cm \times 1 cm fluorimetric quartz cuvette just before the photocatalysis experiments. The concentrations of the catalyst and R6G in the reaction mixture were 50 mg/L and 12.5 μM , respectively.

For the photocatalytic experiments performed under inert conditions, a catalyst suspension in 1:1 (v/v) $\text{CH}_3\text{OH}:\text{H}_2\text{O}$ was placed in a sealed shell-vial and purged with Ar to remove the dissolved oxygen for 30 min. Deaerated TH solution was added to the catalyst suspension just before the photolysis experiment. The concentration of the catalyst in the reaction mixture was 25 mg/L and that of TH was 25 μM .

Photocatalysis was performed with the radiation from a 300 W xenon lamp (Newport Corporation) filtered through a 320 nm high-pass UV filter (Hoya, UV-32). The incident light intensity was set to 0.2 mW/cm². Photolysis was assessed by recording the optical absorbance of the reaction mixture in situ using a USB 4000 fiber optic spectrometer (Ocean Optics). The absorption spectra were recorded over the course of photocatalysis and final results were averaged out of at least 3 independent experiments.

RESULTS AND DISCUSSION

Preparation and Characterization of ZnO–AuNP composites. Carboxylic groups are commonly employed for anchoring of

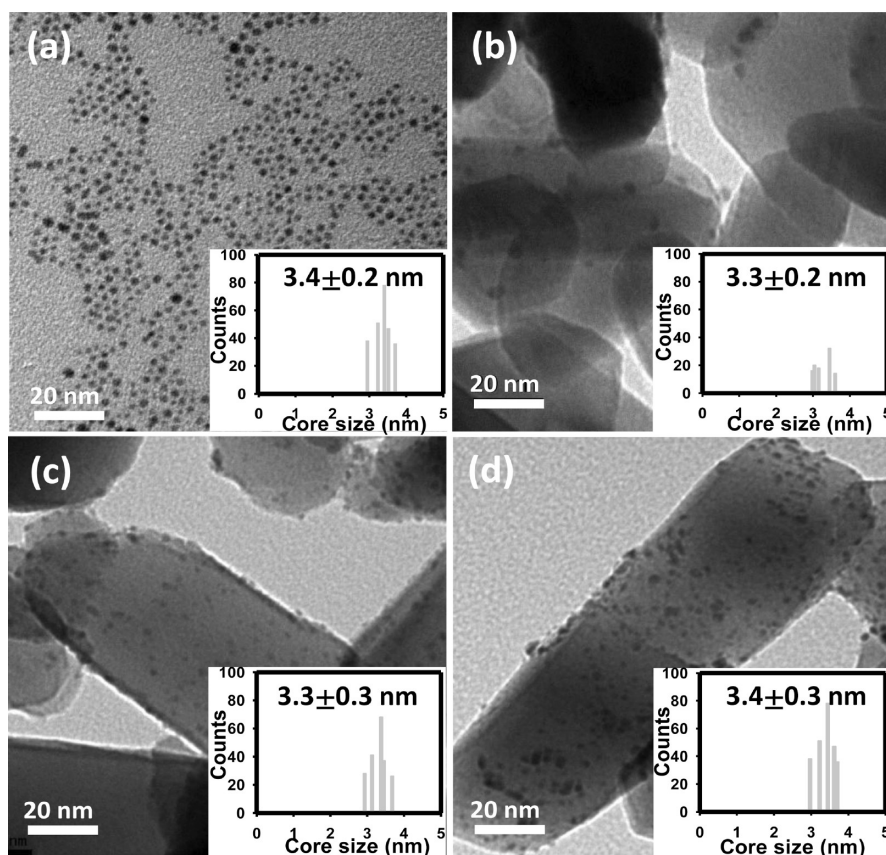


Figure 1. TEM images of (a) glutathione-protected 3.4 nm AuNPs and ZnO-AuNP composites with AuNP loading of (b) 0.4, (c) 1, and (d) 2 wt %. Au cores are darker than the ZnO particles because of the higher electron scattering cross-section of Au. Insets are histograms of Au core diameters.

dye molecules onto metal oxide surfaces. The pH corresponding to the point of zero charge of ZnO is around 9 and thus ZnO carries a net positive charge in neutral, aqueous solutions.²⁵ On the other hand, pK_{a1} and pK_{a2} for the carboxyl groups on the glutathione molecule is 2.1 and 3.5, respectively, and thus the carboxyl groups are expected to exist in the anionic form in a neutral solution.²⁶ Therefore, one can expect a strong electrostatic interaction between the positively charged ZnO surface and the negatively charged carboxyl groups of glutathione molecules. In fact, ZnO-AuNP composites are readily formed by simply stirring of the aqueous mixture of ZnO and AuNP for 5 h without any additives. Figure 1 shows the TEM images of the AuNPs and the ZnO-AuNP composites. The TEM image of the isolated AuNPs shows that the AuNPs are reasonably monodisperse. TEM images of the composites prepared with 0.4, 1, and 2 wt % of AuNPs are shown in parts b, c, and d respectively of Figure 1. It was found that the AuNP anchoring on ZnO readily occurred and thus AuNP loading on ZnO could be conveniently controlled by simply varying the initial concentration of AuNPs in the mixture during the anchoring step. Complete anchoring of AuNPs on ZnO was confirmed by the absence of AuNP absorption from the supernatant of the anchoring solution after separating the ZnO-AuNP composites by centrifugation. TEM images in Figure 1 also shows that all the AuNPs are bound to the surfaces of ZnO and no unbound AuNPs are found after 5 h stirring, proving the effectiveness of this preparation procedure. Importantly, the average AuNP core size was preserved at its initial size of ~ 3.4 nm and no aggregations took place during the binding process.

Optical absorption spectra of ZnO, 2 wt % composite, and AuNP solutions in water are shown in Figure 2a. The absorption maximum at 375 nm of ZnO is comparable to the onset of absorption of macrocrystalline ZnO,²⁷ due to the large average size of ZnO nanoparticles. The AuNPs show a broad absorption near 550 nm that corresponds to the surface plasmon resonance band of gold nanoparticles.²⁸ The absorption profile of the composite is similar to that of ZnO with weak absorption near 550 nm arising from the presence of AuNPs.

PL measurements are widely utilized to characterize semiconductor nanoparticles that exhibit broad range of absorption, narrow emissions with high quantum yields, and size-tunable emission wavelength.^{29–32} On the other hand, gold nanoparticles are known to be effective quenchers when placed in the close proximity to fluorophores.^{33–35} PL emission spectra of ZnO and 2 wt % composite dispersed in water are given in Figure 2b. Emission of ZnO consists of two prominent bands: a narrow emission with a maximum at 377 nm and another broader emission at around 500 nm. The stronger UV emission that corresponds precisely to the absorption band edge can be attributed to the direct radiative recombination of excitons,^{36,37} whereas the broad green emission is commonly assigned to the charge carrier relaxation via surface-related trap states.^{38,39} These trap states are identified as oxygen vacancies on the nanoparticle surface.³⁸

The PL emission of ZnO is seen to be drastically quenched in the presence of AuNPs, showing their strong influence on the charge carrier dynamics. Compared to the emission of ZnO, the 2 wt % composite exhibits significantly weaker, featureless emission

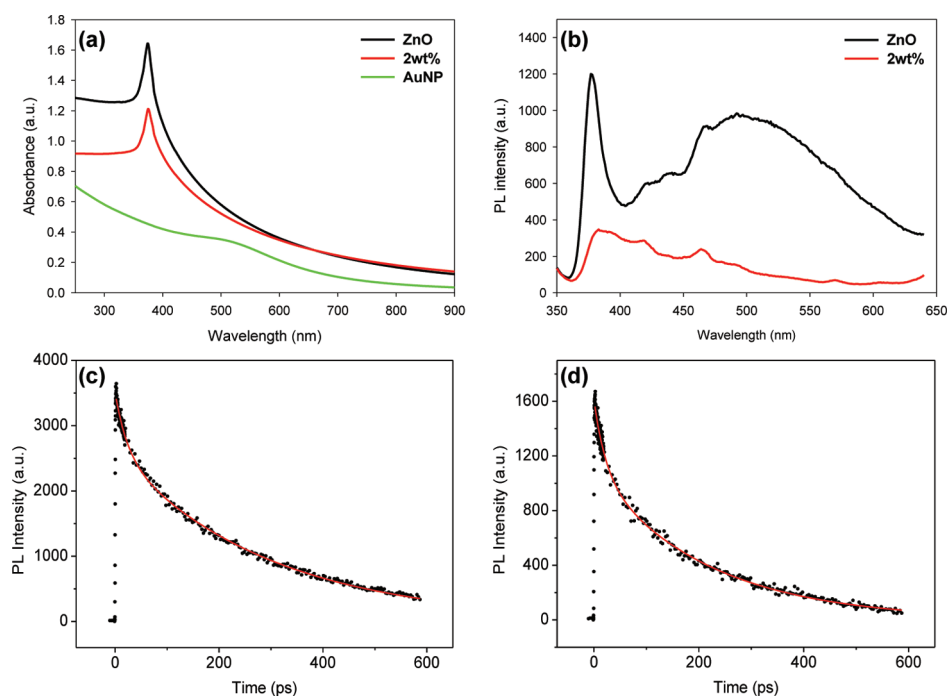


Figure 2. (a) Optical absorption spectra of ZnO, 2 wt % composite, and AuNP solutions in water. (b) PL spectra of ZnO and 2 wt % composite suspension in water. PL decay profiles with the corresponding biexponential fits for (c) ZnO and (d) 2 wt % composite.

Table 1. Time Constants (τ) and Relative Amplitudes (a) from Bi-Exponential Fits to the PL Decay Profiles of ZnO and 2 wt % Composite Dispersions in Water

catalysts	a_1	τ_1 (ps)	a_2	τ_2 (ps)
ZnO	25.5	23.3	74.5	293
2 wt % composite	32.3	22.3	67.7	215

with a maximum around 383 nm. UV emission was found to be reduced by 71%, whereas the drop in visible emission was 84%, which illustrates that the AuNPs block both direct and trap-related charge carrier recombination pathways. This result suggests that AuNPs on ZnO surface are able to extract electrons from the conduction band of ZnO and thus prevent charge carrier recombination within the ZnO nanoparticles.

To further understand the charge transfer process between ZnO and AuNPs, PL lifetimes of the band edge emission were measured at 375 nm using a 267 nm laser as the excitation source. The experiments were carried out in aerated samples so that no charge accumulation occurred during UV irradiation. The PL lifetime depends upon both the radiative and nonradiative processes and thus its change can reveal a particular deactivation process.⁴⁰ In the present study, the PL lifetime of ZnO can be used to investigate the charge transfer deactivation process occurring in the composites. Panels c and d in Figure 2 show the PL decay profiles from ZnO and 2 wt % composite, respectively. The experimental decay profiles were fitted using a nonlinear least-squares method with a two-component decay model. Table 1 summarizes the time constants and relative amplitudes from the biexponential fits.

Comparing with the lifetime results reported by Xiong et al.⁴¹ for ZnO nanoparticles with sizes ranging 25–73 nm, the fast decay component (τ_1) in Table 1 can be attributed to nonradiative

recombination of near surface excitons and the slow component (τ_2) to the radiative recombination of the free excitons.^{42,43} Whereas the fast decay lifetime is rather insensitive to the presence of AuNPs, the slow component appears to be considerably affected by the presence of AuNPs. The PL lifetime (τ_2) of the 2 wt % composite is 215 ps, significantly shortened in the presence of AuNPs, compared to that of ZnO (293 ps). This result suggests that the presence of AuNPs on ZnO surface provides an additional deactivation pathway corresponding to the electron transfer from ZnO to AuNPs, leading to a significant decrease in the PL lifetime. We can estimate the electron transfer rate constant (k_{ET}) by comparing the PL lifetime of ZnO in the presence of and absence of AuNP:

$$k_{ET} = 1/\tau_{(ZnO-AuNP)} - 1/\tau_{(ZnO)} \quad (1)$$

The rate constant of $\sim 1.2 \times 10^9 \text{ s}^{-1}$ calculated using τ_2 of ZnO and 2 wt % composite reflects the electron transfer time scale of ~ 830 ps in the ZnO-AuNP composite. The comparison of the PL lifetimes also reveals that the electron transfer from the excited ZnO to AuNPs accounts for ca. 27% of deactivation processes for 2 wt % composite.⁴⁴ On the basis of the steady-state and time-resolved PL results, it can be concluded that the AuNPs present on the surface of ZnO effectively block both direct and trap-related charge carrier recombination pathways by extracting electrons from the photoexcited ZnO. The transferred electrons may subsequently be used for catalytic reactions, which could lead to the significant enhancement of the photocatalytic activity of the ZnO-AuNP composites (vide infra).

Photocatalytic Degradation of Rhodamine 6G (R6G). The photocatalytic activity of the composites was examined by monitoring the degradation of R6G dye in aqueous medium. Evolution of the absorption profiles during the photocatalytic degradation of R6G with ZnO and the 2 wt % composite are shown in

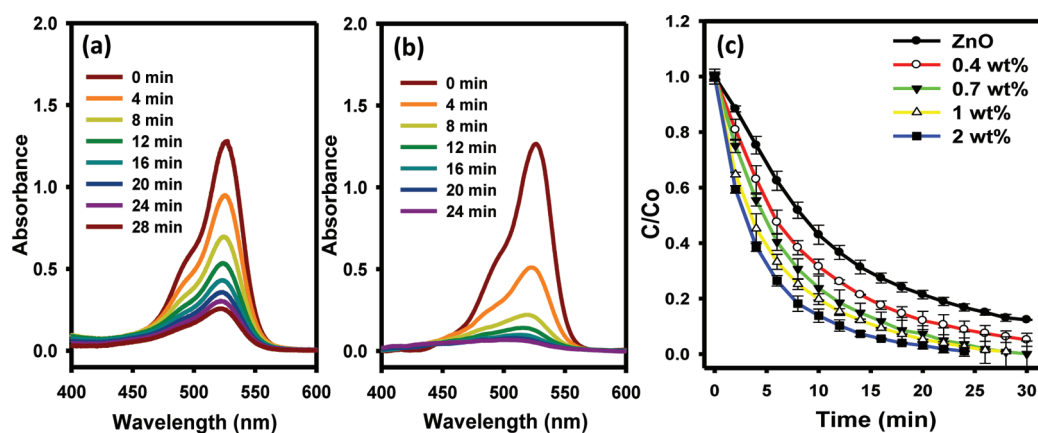


Figure 3. Temporal evolution of absorption spectra obtained during photocatalysis of R6G with (a) ZnO, (b) 2 wt % composite, and (c) change in R6G concentration (C) relative to the initial concentration (C_0) during photocatalysis with ZnO and the composites with different AuNP loadings (0.4, 0.7, 1, and 2 wt %). The R6G concentration was estimated from the absorbance at 525 nm.

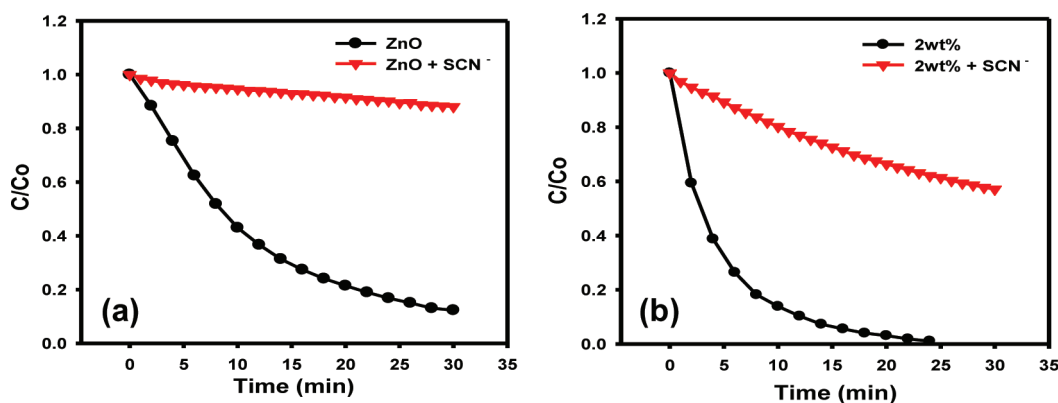


Figure 4. Effect of SCN^- on R6G photocatalysis with (a) ZnO and (b) 2 wt % composite. $[\text{SCN}^-] = 137 \mu\text{M}$.

parts a and b of Figure 3. As can be seen in the figures, both ZnO and the composite show similar changing patterns of the absorption profiles, which suggests that the R6G degradation occurs via a similar pathway. The composite exhibits, however, much faster decomposition rate compared to ZnO; that is, during the 30 min photolysis the composite was able to completely bleach the dye, while ZnO only resulted in a partial decomposition. To compare the photocatalytic activity more quantitatively, we monitored the changes in R6G concentration (C) relative to the initial concentration (C_0) during photocatalysis. The R6G concentration was estimated from the absorbance at 525 nm. As shown in Figure 3c, the photolysis time corresponding to 50% degradation of R6G is ~ 8 min with ZnO. The catalytic activity increases significantly with AuNP loading; the 50% photolysis time decreases to ~ 6 min with 0.4 wt % composite and further decreases to ~ 2.5 min as the AuNP loading increases to 2 wt %. This result clearly demonstrates the positive role of AuNP in the photocatalytic activity of the composite with which the photocatalytic activity increases with AuNP loading. Gold nanoparticles are known to be a strong light absorber and thus light screening effect may in effect at higher gold loading, which would result in decrease in the photocatalytic activity at higher gold loadings.^{8,45} In the present study, however, such a decrease was not observed from the composites with AuNP loading up to 2 wt %, presumably because of relatively low loadings examined.

Additionally, the results show that regardless of the catalyst used, the dye absorption is bleached throughout the observed spectral region, which may be indicative of full decomposition. Further testing revealed that the bleaching of R6G was not reversible. These observations suggest a permanent mineralization of the dye during this photolysis.

Although the photobleaching of R6G can occur via oxidative or reductive pathway,⁴⁶ the irreversible mineralization of R6G suggests that it occurs via oxidative pathway by the photogenerated holes. It has been well-documented that the photogenerated holes play an important role in a number of photocatalytic processes.^{47,48} To examine the role of the valence band holes in the photocatalytic degradation of R6G, we carried out photocatalysis of the dye in the presence of a known hole scavenger, thiocyanate ion.⁴⁹ The degradation profiles of R6G in the presence of SCN^- are shown in Figure 4, where R6G degradation is found to be strongly inhibited by the presence of SCN^- for both ZnO and 2 wt % composite as the catalyst. Therefore, it can be concluded that the valence band holes are directly accountable for the degradation of R6G in the present catalytic system. It is interesting to note that the inhibition by SCN^- is found to be less significant and there is still considerable photocatalytic activity observed with the composite catalyst even in the presence of SCN^- . This result indicates that the charge separation in ZnO is sufficiently enhanced by the modification with

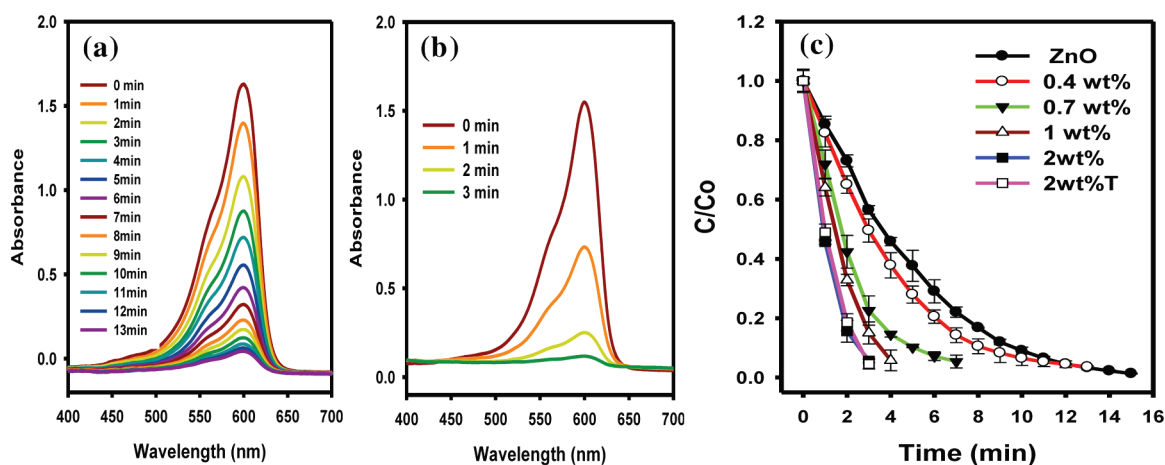


Figure 5. Temporal evolution of absorption spectra obtained during photolysis of TH with (a) ZnO, (b) 2 wt % composite, and (c) change in TH concentration (C) relative to the initial concentration (C_0) during photocatalysis with ZnO and the composites with different AuNP loadings (0.4, 0.7, 1, and 2 wt %) and thermally treated 2 wt % composite (2 wt % T). The TH concentration was estimated from the absorbance at 600 nm.

AuNPs, which results in higher availability of holes in the composite compared to ZnO.

Photocatalytic Degradation of Thionine (TH). In addition to the valence band holes, the photogenerated conduction band electrons of the ZnO nanoparticles possess a strong reductive power that is related to the conduction band position of the semiconductor.⁵⁰ The reductive power of the composite photocatalyst was probed using TH dye. In order to study the catalytic activity by the photogenerated electrons alone, the experiments were conducted in the absence of the photogenerated holes using CH_3OH , an effective hole scavenger.⁵¹ Additionally, the photocatalytic reaction was performed in the absence of oxygen, in order to avoid electron scavenging by oxygen dissolved in the solution.⁵² As illustrated in Scheme 1, band gap illumination of ZnO in deaerated $\text{CH}_3\text{OH-H}_2\text{O}$ generates electrons in the conduction band while holes are scavenged by CH_3OH . The band energy positions of ZnO are similar to those of TiO_2 .⁵³ It is therefore expected that the photoelectrons generated in the conduction band of ZnO can readily transfer to the attached AuNPs in the composite, as has been observed in the TiO_2 -AuNP composites.^{16,34} Consequently, charge separation in the composites can be greatly enhanced in the presence of AuNPs and thus more photoelectrons will be available for the catalytic reduction of TH.

The evolution of the optical absorption profile of the reaction mixture during the photocatalytic degradation of TH with ZnO and the 2 wt % composite are compared in parts a and b of Figure 5. It can be seen that the absorption of TH, with a maximum at 600 nm, is rapidly bleached in the presence of either catalyst. However, rate of photolysis is greatly enhanced with the composite. In Figure 5c, photolysis time corresponding to 50% degradation of TH is 3.7 min with ZnO. For composites, the photolysis time dramatically decreases with increasing AuNP loading; the photolysis time decreased to 3.0, 1.7, 1.4, and 0.9 min with 0.4, 0.7, 1, and 2 wt % composite. As was observed for R6G photocatalysis, the strongest enhancement of the activity was observed with the highest AuNP loading (i.e., 2 wt % composite). The clear correlation between the AuNP loading and the photocatalytic activity observed here undoubtedly demonstrates the active role of AuNP in the photocatalytic reduction of TH.

The dramatic enhancement of the photocatalytic activity by the modification of AuNPs found in ZnO-AuNP composites is in sharp contrast to the previous result observed for TiO_2 -AuNP composites.¹⁶ In our previous study,¹⁶ it was found that the photocatalytic activity of TiO_2 nanoparticles exhibit essentially no enhancement when modified with gold nanoparticles. The catalytic activity of the composites was enhanced only after thermal treatment. This result suggested that the presence of ligands on gold nanoparticles imposed a large kinetic barrier for electron transfer from TiO_2 to gold nanoparticle and thus the charge separation and the catalytic activity were enhanced only after removing the ligand via thermal treatment. The reason for the contrasting result observed for the two composite systems is unclear at this juncture, but it could be associated with the difference in catalytic reactivity between TiO_2 and ZnO and/or the difference in the electron transfer dynamics between metal oxide and AuNP. Comparative dynamics study will be needed to fully understand the origin of the difference in these composite systems. This will be pursued in future work.

Finally, the composite was thermally treated at 250 °C for 30 min to see whether its catalytic activity could be enhanced after the removal of the glutathione ligand, as was observed for TiO_2 -AuNP composites.^{16,17} The temperature was set to 250 °C because ZnO exhibited activity change when thermally treated above 300 °C. The TEM image shown in Figure S1 (see the Supporting Information) shows that the gold particles are still well dispersed on ZnO surface and the average size of the particles (3.6 nm) is almost unchanged after the thermal treatment, highlighting the advantage of the present method for the composite formation. The thermogravimetric analysis (TGA) result in Figure S2 (see the Supporting Information) suggests that the glutathione ligand is partially removed by the thermal treatment at 250 °C. Nevertheless, significant removal of the ligand is expected by the thermal treatment and thus it should be possible to examine the ligand effect on the catalytic activity of the composite. As can be seen in Figure 5(c), the catalytic activity of the thermally treated composite (2 wt % T) is essentially the same as that of the untreated composite (2 wt %), indicating that the presence of ligand between ZnO and AuNP has little influence on the catalytic activity. This result also implies that the electron transfer through the linker ligand occurs at a relatively

shorter time scale than that of the catalytic reduction of TH and thus the composite exhibits little enhancement in the catalytic activity after the thermal treatment.

CONCLUSIONS

A well-defined nanoparticle-based photocatalytic system was developed with ZnO and thiolate-protected AuNPs using a facile method. The method is highly versatile in that the ZnO–AuNP composites can be prepared in well-defined forms, as bifunctional glutathione protected AuNPs with high monodispersity are utilized and the extent of AuNP loading is precisely controlled. Assembly of AuNPs on ZnO surfaces caused a strong quenching of ZnO photoluminescence, signifying the ability of AuNPs to effectively inhibit charge recombination and direct the charge carriers to interfacial reactions. This characteristic was further established by the PL lifetime results of ZnO, where a considerable decrease in the PL decay constants confirmed the additional nonradiative electron transfer pathway in the presence of AuNPs. The composites were found to exhibit strongly enhanced photocatalytic activity without requiring any thermal activation step for both photooxidation and photoreduction reactions. A clear correlation between the photocatalytic activity and the AuNP loading was observed for both reactions. These results demonstrate that thiolate-protected AuNPs can effectively enhance the charge separation by extracting electrons from the photoexcited ZnO, and consequently improve the efficiency of the photocatalytic reactions. The combination of well-defined gold nanoparticles with metal oxide photocatalysts could open the avenue to develop tunable photocatalysts whose reactivity can be controlled by the size, shape, and loading of gold nanoparticles.

ASSOCIATED CONTENT

S Supporting Information. TEM image of 2 wt % composite thermally treated at 250 °C and TGA of glutathione-protected AuNPs. This material is available free of charge via the Internet at <http://pubs.acs.org>.

AUTHOR INFORMATION

Corresponding Author

*E-mail: dongil@yonsei.ac.kr. Telephone: (82-2)-2123-5638. Fax: (82-2)-364-7050.

ACKNOWLEDGMENT

This research was supported by the Mid-Career Researcher Program (2011-0029735), Basic Science Research Program (2010-0009244), World Class University Program (R32-2008-000-10217-0), and Priority Research Centers Program (2009-0093823) through NRF grant funded by the Ministry of Education, Science and Technology, and Yonsei University Research Fund. N.U. is thankful for the financial support from Western Michigan University. The authors thank Prof. Guda Ramakrishna for help with time-resolved PL experiments.

REFERENCES

- (1) Fujishima, A.; Honda, K. *Nature* **1972**, *238*, 37–38.
- (2) Serpone, N.; Lawless, D.; Khairutdinov, R. *J. Phys. Chem.* **1995**, *99*, 16646.
- (3) Hoffman, A. J.; Carraway, E. R.; Hoffmann, M. R. *Environ. Sci. Technol.* **1994**, *28*, 776–785.
- (4) Anpo, M.; Aikawa, N.; Kubokawa, Y. *J. Phys. Chem.* **1984**, *88*, 3998–4000.
- (5) Nedeljkovic, J. M.; Nenadovic, M. T.; Micic, O. I.; Nozik, A. J. *J. Phys. Chem.* **1986**, *90*, 12–13.
- (6) Kamat, P. V. *J. Phys. Chem. C* **2007**, *111*, 2834–2860.
- (7) Kamat, P. V.; Barazzouk, S.; Hotchandani, S. *Angew. Chem., Int. Ed.* **2002**, *41*, 2764–2767.
- (8) Kamat, P. V. *J. Phys. Chem. B* **2002**, *106*, 7729–7744.
- (9) Serp, P.; Kalck, P.; Feurer, R. *Chem. Rev.* **2002**, *102*, 3085–3128.
- (10) Venezia, A. M.; Pantaleo, G.; Longo, A.; Di Carlo, G.; Casaletto, M. P.; Liotta, F. L.; Deganello, G. *J. Phys. Chem. B* **2005**, *109*, 2821–2827.
- (11) Oh, H. S.; Yang, J. H.; Costello, C. K.; Wang, Y. M.; Bare, S. R.; Kung, H. H.; Kung, M. C. *J. Catal.* **2002**, *210*, 375–386.
- (12) Wolf, A.; Schüth, F. *Appl. Catal., A* **2002**, *226*, 1–13.
- (13) Daniel, M.-C.; Astruc, D. *Chem. Rev.* **2003**, *104*, 293–346.
- (14) Valden, M.; Lai, X.; Goodman, D. W. *Science* **1998**, *281*, 1647–1650.
- (15) Zheng, N.; Fan, J.; Stucky, G. D. *J. Am. Chem. Soc.* **2006**, *128*, 6550–6551.
- (16) Lee, M.; Amaratunga, P.; Kim, J.; Lee, D. *J. Phys. Chem. C* **2010**, *114*, 18366–18371.
- (17) Amaratunga, P.; Lee, M.; Kim, J.; Lee, D. *Can. J. Chem.* **2011**, *89*, 1001–1009.
- (18) Chu, D.; Masuda, Y.; Ohji, T.; Kato, K. *Langmuir* **2010**, *26*, 2811–2815.
- (19) Kislov, N.; Lahiri, J.; Verma, H.; Goswami, D. Y.; Stefanakos, E.; Batzill, M. *Langmuir* **2009**, *25*, 3310–3315.
- (20) Chou, T. P.; Zhang, Q.; Fryxell, G. E.; Cao, G. *Adv. Mater.* **2007**, *19*, 2588–2592.
- (21) Zheng, N.; Stucky, G. D. *J. Am. Chem. Soc.* **2006**, *128*, 14278–14280.
- (22) Comotti, M.; Li, W.-C.; Spliethoff, B.; Schüth, F. *J. Am. Chem. Soc.* **2005**, *128*, 917–924.
- (23) Templeton, A. C.; Chen, S.; Gross, S. M.; Murray, R. W. *Langmuir* **1998**, *15*, 66–76.
- (24) Devadas, M. S.; Kwak, K.; Park, J.-W.; Choi, J.-H.; Jun, C.-H.; Sinn, E.; Ramakrishna, G.; Lee, D. *J. Phys. Chem. Lett.* **2010**, *1*, 1497–1503.
- (25) Parks, G. A. *Chem. Rev.* **1965**, *65*, 177–198.
- (26) Armas, M. T.; Mederos, A.; Gili, P.; Domínguez, S.; Hernández-Molina, R.; Lorenzo, P.; Baran, E. J.; Araujo, M. L.; Brito, F. *Polyhedron* **2001**, *20*, 799–804.
- (27) Haase, M.; Weller, H.; Henglein, A. *J. Phys. Chem.* **1988**, *92*, 482–487.
- (28) Eustis, S.; El-Sayed, M. A. *Chem. Soc. Rev.* **2006**, *35*, 209–217.
- (29) Nirmal, M.; Brus, L. *Acc. Chem. Res.* **1998**, *32*, 407–414.
- (30) Wu, X.; Liu, H.; Liu, J.; Haley, K. N.; Treadway, J. A.; Larson, J. P.; Ge, N.; Peale, F.; Bruchez, M. P. *Nat. Biotechnol.* **2003**, *21*, 41–46.
- (31) Alivisatos, A. P. *Science* **1996**, *271*, 933–937.
- (32) Gill, R.; Zayats, M.; Willner, I. *Angew. Chem., Int. Ed.* **2008**, *47*, 7602–7625.
- (33) Huang, T.; Murray, R. W. *Langmuir* **2002**, *18*, 7077–7081.
- (34) Kim, J.; Lee, D. *J. Am. Chem. Soc.* **2007**, *129*, 7706–7707.
- (35) Kondon, M.; Kim, J.; Udawatte, N.; Lee, D. *J. Phys. Chem. C* **2008**, *112*, 6695–6699.
- (36) Hu, Y.; Jiang, Z.; Xu, C.; Mei, T.; Guo, J.; White, T. *J. Phys. Chem. C* **2007**, *111*, 9757–9760.
- (37) Yang, C. L.; Wang, J. N.; Ge, W. K.; Guo, L.; Yang, S. H.; Shen, D. Z. *J. Appl. Phys.* **2001**, *90*, 4489–4493.
- (38) Vanheusden, K.; Warren, W. L.; Seager, C. H.; Tallant, D. R.; Voigt, J. A.; Gnade, B. E. *J. Appl. Phys.* **1996**, *79*, 7983–7990.
- (39) Kohan, A. F.; Ceder, G.; Morgan, D.; Van de Walle, C. G. *Phys. Rev. B* **2000**, *61*, 15019.
- (40) Love, L. J. C.; Shaver, L. A. *Anal. Chem.* **1976**, *48*, 364A.
- (41) Xiong, G.; Pal, U.; Serrano, J. G. *J. Appl. Phys.* **2007**, *101*, 024317–6.
- (42) Huang, M. H.; Mao, S.; Feick, H.; Yan, H.; Wu, Y.; Kind, H.; Weber, E.; Russo, R.; Yang, P. *Science* **2001**, *292*, 1897–1899.

- (43) Hong, S.; Joo, T.; Park, W. I.; Jun, Y. H.; Yi, G.-C. *Appl. Phys. Lett.* **2003**, *83*, 4157–4159.
- (44) Halder, K. K.; Sen, T.; Patra, A. *J. Phys. Chem. C* **2008**, *112*, 11650–11656.
- (45) Tada, H.; Teranishi, K.; Inubushi, Y.-I.; Ito, S. *Langmuir* **2000**, *16*, 3304–3309.
- (46) Aarthi, T.; Madras, G. *Ind. Eng. Chem. Res.* **2007**, *46*, 7–14.
- (47) Bandara, J.; Mielczarski, J. A.; Kiwi, J. *Langmuir* **1999**, *15*, 7680–7687.
- (48) Konstantinou, I. K.; Albanis, T. A. *Appl. Catal., B* **2004**, *49*, 1–14.
- (49) Bahnemann, D. W.; Hilgendorff, M.; Memming, R. *J. Phys. Chem. B* **1997**, *101*, 4265–4275.
- (50) Staniszewski, A.; Morris, A. J.; Ito, T.; Meyer, G. J. *J. Phys. Chem. B* **2007**, *111*, 6822–6828.
- (51) Wood, A.; Giersig, M.; Mulvaney, P. *J. Phys. Chem. B* **2001**, *105*, 8810–8815.
- (52) Sun, Y.; Pignatello, J. J. *Environ. Sci. Technol.* **1995**, *29*, 2065–2072.
- (53) Graetzel, M. *Nature* **2001**, *414*, 338–344.